First-Principles Mode Gruneisen Parameters and Negative Thermal Expansion in α-ZrW_2O_8

V. Gava, A. L. Martinotto, and C. A. Perottoni*

Instituto de Materiais Cerâmicos, Universidade de Caxias do Sul, 95765-000 Bom Princípio–Rio Grande do Sul, Brazil

(Received 18 May 2012; revised manuscript received 16 September 2012; published 7 November 2012)

Mode Grüneisen parameters were estimated for α-ZrW_2O_8 zone-center modes by means of density functional theory calculations and the temperature dependence of the coefficient of thermal expansion was obtained according to the Debye-Einstein model of the quasiharmonic approximation. The lowest energy optic modes were identified at 45 and 46 cm^{-1}, and were shown to be the main modes responsible for negative thermal expansion at low temperature. Experimental evidence of the lowest energy, triply degenerated infrared active optic mode, was also found in the far infrared spectrum of α-ZrW_2O_8. Upon increasing temperature, other optic modes with $E < 25$ meV (particularly at 96, 100, 133, 161, and 164 cm^{-1}) also contribute significantly to the coefficient of thermal expansion near room temperature. An analysis was made of selected zone-center modes in light of previously proposed models for explaining negative thermal expansion in open framework materials.

DOI: 10.1103/PhysRevLett.109.195503 PACS numbers: 63.20.dk, 62.50.−p, 65.40.De

Negative thermal expanssion (NTE) in zirconium tungstate was first reported by Martinek and Hummel in 1968 [1], almost ten years after this compound was synthesized by Graham *et al.* [2]. However, it was only after the discovery that α-ZrW_2O_8 exhibits NTE over a wide temperature range (0.3 to 1050 K) that interest in this compound resurged in 1996 [3]. At ambient conditions, α-ZrW_2O_8 exhibits a metastable cubic structure (space group $P2_13$), which can be described as a tridimensional arrangement of corner-sharing ZrO_6 octahedra and WO_4 tetrahedra. Of the four O atoms in the first coordination polyhedra around tungsten, only three are shared with neighbor Zr atoms. The fourth oxygen, bonded only to W, is termed the terminal oxygen. The terminal oxygen confers great flexibility to the α-ZrW_2O_8 framework. Indeed, the standard mechanism proposed for explaining NTE in α-ZrW_2O_8 is based on rigid unit modes (RUMs) involving the coordinate rotation of ZrO_6 and WO_4 polyhedra [4,5]. Evidence for this low-energy lattice dynamics has been found in inelastic neutron scattering experiments, low-temperature specific heat measurements, and in the temperature dependence of the α-ZrW_2O_8 lattice parameter [6–8]. However, despite the success of this simple model in capturing the essential features behind NTE in α-ZrW_2O_8, the precise nature of the vibrational modes responsible for NTE in α-ZrW_2O_8 remains controversial.

Previous studies based on the analysis of low temperature heat capacity measurements have suggested that a weakly dispersive optic mode with energy around 5 meV (40 cm^{-1}), possibly associated with the large-amplitude motion of terminal oxygens, is responsible for NTE in α-ZrW_2O_8 [7]. This conclusion received further support from the analysis of the dependence on temperature of the α-ZrW_2O_8 lattice parameter, which suggested that NTE in α-ZrW_2O_8 is caused by RUMs with energies between 3 and 8 meV, with a significant contribution peaking at 4.7 meV (38 cm^{-1}) [8]. Accordingly, a Raman peak observed at 40 cm^{-1} was attributed as being mainly responsible for NTE in α-ZrW_2O_8 [9,10]. On the other hand, the analysis of infrared reflectivity results [11] pointed to a lowest energy optic mode at 28 cm^{-1}, which presumably should contribute significantly to NTE in zirconium tungstate.

Later on, inelastic neutron scattering measurements led to the observation of an unusual phonon softening upon pressure increase and, thus, large negative Gruneisen parameters for phonons with $E < 8$ meV (65 cm^{-1}) [12]. This observation also received support from lattice dynamical calculations based on empirical interatomic potentials [13]. However, a controversy arose after high pressure Raman spectroscopy results showed evidence of several modes with $E < 50$ meV (400 cm^{-1}) exhibiting negative Gruneisen parameters [14–16].

Further experimental evidence on the microscopic mechanism behind NTE in α-ZrW_2O_8 resulted from the analysis of x-ray absorption fine structure (XAFS) data by Cao *et al.* [17,18]. Based on the observation that the Zr $\cdots$ W peaks in the Fourier transform of the zirconium tungstate XAFS spectra have a very small temperature dependence, Cao *et al.* proposed that the Zr–O–W linkage should be stiff enough to form a quasirigid unit consisting of WO_4 and the three nearest ZrO_6 octahedra. Accordingly, NTE in α-ZrW_2O_8 was attributed to the translational motion of WO_4 tetrahedra along the $\langle 111 \rangle$ axis and the correlated motion of the three nearest ZrO_6 octahedra (tent model). The mixed librational and translational character of the low-energy modes involved in the mechanism behind NTE in zirconium tungstate was later also inferred from the analysis of infrared reflectivity data [11]. In contrast, Tucker *et al.* [19] concluded, on the basis of a reverse Monte Carlo analysis of neutron total scattering data for α-ZrW_2O_8, that NTE results from RUMs

involving the correlated rotation of the metal-oxygen polyhedra and that a rigid Zr–O–W linkage would have the effect of stiffening the structure, thus inhibiting NTE in zirconium tungstate.

The disagreement about the frequency of the lowest energy optic mode, the nature of the low-energy modes responsible for NTE in α-ZrW_2O_8, and the role played by modes with $E > 10$ meV in the mechanism behind this phenomenon points to the need for a thorough lattice dynamical study. Accordingly, in this work, density functional theory (DFT) calculations were carried out to determine the mode Grüneisen parameters for all the 54 inequivalent zone-center optic modes of α-ZrW_2O_8. From these, the linear coefficient of thermal expansion (CTE) was obtained according the Debye-Einstein model of the quasiharmonic approximation (QHA) [20–23].

All calculations were performed in the athermal limit, with the CRYSTAL06 computer code [24]. The crystalline orbitals were each expressed as a sum of atom-centered Gaussian functions over all equivalent sites. Total energies were evaluated according to density functional theory, with the Becke three-parameter Lee-Yang-Parr hybrid functional (B3LYP) gradient-corrected hybrid exchange-correlation density functional [25]. The basis sets were the same previously used to calculate the α-ZrW_2O_8 elasticity tensor near 0 K [26]. Details of these calculations are given in the Supplemental Material [27].

Calculations in the quasiharmonic approximation were performed according to the Debye-Einstein model, where the contribution of acoustic branches was treated according the Debye model and the $3N - 3$ optic branches were accounted for by a sum over Einstein terms. Previously calculated elastic constants at 0 K were used for estimating the Poisson ratio ($\nu = 0.318$). The corresponding Debye temperature and acoustic Grüneisen parameter ($\gamma_{ac} = 1.92$) were obtained according to Fleche [22]. The mode frequencies calculated at the Γ point were taken as representative of the whole optic branch. However, instead of the usual approximation of considering just a single overall optic Grüneisen parameter, individual mode Grüneisen parameters (γ_i) were used for every single optic mode in the QHA calculations. At zero pressure, the unit cell volume as a function of temperature was found by solving

$$P = P_{sta} + \frac{k_B T}{V}\left\{\gamma_{ac}\left[\frac{9}{8}\left(\frac{\theta_D}{T}\right) + 3D\left(\frac{\theta_D}{T}\right)\right] + \sum_{i=1}^{3N-3} \gamma_i x_i \left(\frac{1}{2} + \frac{1}{e^{x_i} - 1}\right)\right\}, \quad (1)$$

where P_{sta} is the static pressure given by Murnaghan equation, V is the unit cell volume, k_B is the Boltzmann constant, D is the Debye integral, θ_D is the Debye temperature, and $x_i = \theta_{Ei}/T$, where $\theta_{Ei} = E_i/k_B$ is the Einstein temperature for the ith vibrational mode with energy E_i. The summation extends over all the $3N - 3 = 129$ (54 inequivalent) vibrational modes of the 44 atoms in the α-ZrW_2O_8 unit cell.

In order to provide further experimental information on the low energy modes presumably responsible for NTE in zirconium tungstate, far infrared absorption spectroscopy was performed using a PerkinElmer Spectrum 400 Fourier transform spectrometer. A fine powder sample of zirconium tungstate (Wah Chang Co., Albany, OR), previously heated to 200 °C for two hours (to remove any residual moisture and also to convert to α-ZrW_2O_8 a small amount of γ-ZrW_2O_8 present in the sample as received), was gently pressed by hand in a steel die to form a self-supporting disk with 70 μm thickness. A transmission spectrum comprising 1200 scans, collected with 4 cm^{-1} resolution, is shown in Fig. 1.

The equilibrium lattice parameter at 0 K, 9.3525(27) Å, and the bulk modulus and its first pressure derivative, 99.3(4) GPa and 4.2(2), respectively, agree within the uncertainties of the fitting with previous results [26]. The variation of total energy versus primitive cell volume for α-ZrW_2O_8, and a comparison of the equilibrium lattice parameter and optimized atomic positions with experimental data from high-resolution powder diffraction at 2 K can be found in the Supplemental Material [27].

Factor group analysis yields the decomposition in irreducible representations of the α-ZrW_2O_8 optic modes according to 11A + 11E + 32F. All the optic modes are Raman active, but only the 32F modes are also IR active. Theoretical mode frequencies and mode Grüneisen parameters are given in Table I.

The theoretical lowest energy optic IR active mode, at 45 cm^{-1}, is in good agreement with a strong absorption band observed at 40 cm^{-1} in the room temperature far infrared spectrum of α-ZrW_2O_8, and also with a peak in the α-ZrW_2O_8 optic conductivity spectrum [11]. Both the first and the second lowest energy modes, this latter at 46 cm^{-1}, are also consistent with experimental data from Raman scattering [9,10,14]. Our calculations give support to the interpretation by Hancock *et al.* [11] that the 20 cm^{-1} peak in the optic conductivity spectrum of

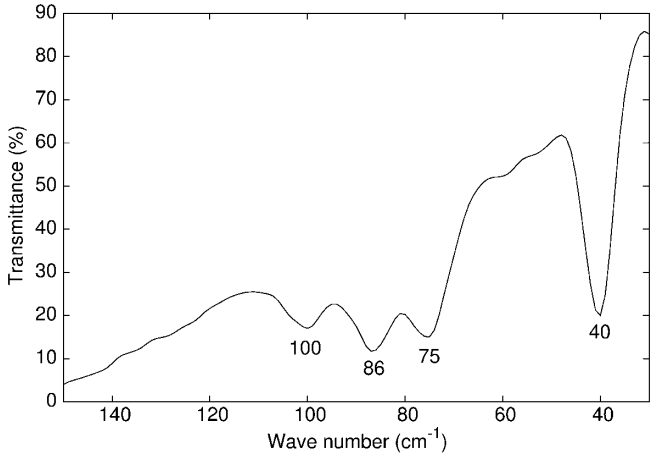

FIG. 1. Far infrared spectrum of α-ZrW_2O_8 and wave numbers of some of the more prominent absorption bands.

TABLE I. Mode number, calculated mode frequencies, and mode Grüneisen parameters for α-ZrW_2O_8. (A), (E), and (F) stand for singly, doubly, and triply degenerated modes, respectively.

Mode #	ν (cm^{-1})	γ	Mode #	ν (cm^{-1})	γ
1	45(F)	−4.8	28	307(F)	−0.3
2	46(E)	−4.2	29	315(F)	−0.4
3	59(A)	−0.6	30	320(E)	−0.5
4	75(F)	−2.0	31	322(F)	−0.3
5	96(F)	−3.4	32	338(F)	−0.4
6	97(A)	3.1	33	356(E)	0.4
7	100(F)	−2.2	34	357(A)	0.1
8	111(F)	2.2	35	359(F)	0.0
9	122(E)	−1.7	36	371(F)	−0.3
10	133(F)	−4.3	37	382(F)	0.2
11	155(A)	−0.6	38	403(F)	0.2
12	161(F)	−2.5	39	405(E)	0.3
13	164(E)	−2.0	40	416(F)	0.3
14	172(E)	0.6	41	734(F)	1.7
15	179(F)	0.8	42	738(E)	1.7
16	191(F)	0.6	43	769(F)	1.4
17	198(F)	−0.8	44	818(E)	1.3
18	210(F)	−0.9	45	819(F)	1.3
19	233(F)	1.0	46	853(A)	1.0
20	246(A)	−1.0	47	859(F)	1.0
21	247(E)	1.3	48	905(F)	0.6
22	256(F)	0.2	49	921(A)	0.2
23	280(A)	−0.6	50	998(F)	0.7
24	281(F)	0.2	51	1016(F)	1.1
25	286(F)	0.4	52	1022(A)	0.7
26	300(A)	−0.2	53	1025(F)	0.8
27	303(E)	−0.6	54	1030(A)	0.9

zirconium tungstate does not correspond to a zone-center optic mode. However, the DFT results show no evidence of any vibrational mode that could be assigned to the broad band at 28 cm^{-1}, previously identified as the lowest optic phonon [11]. Besides the modes at 45 and 46 cm^{-1}, other optic modes at 96, 100, 133, 161, and 164 cm^{-1} also exhibit negative mode Grüneisen parameters. The 96 cm^{-1} mode can be tentatively assigned to a Raman peak observed at 84 cm^{-1}, which was reported as exhibiting a negative mode Grüneisen parameter [11,14]. Results from complementary plane wave pseudopotential calculations [27] suggest the existence of strong infrared bands at 43, 79, 91, and 109 cm^{-1}, in good agreement with the bands in the far infrared spectrum shown in Fig. 1. The corresponding modes in the Becke three-parameter Lee-Yang-Parr hybrid functional density functional theory calculations are found at 45, 100, 111, and 133 cm^{-1}. The agreement between experimental and plane wave pseudopotential frequencies becomes worse for the high energy, internal modes, for which frequencies originally calculated using atom-centered basis sets compare better to experimental results. The tendency to overestimate frequencies is a known issue with DFT calculations [28]. It is expected,

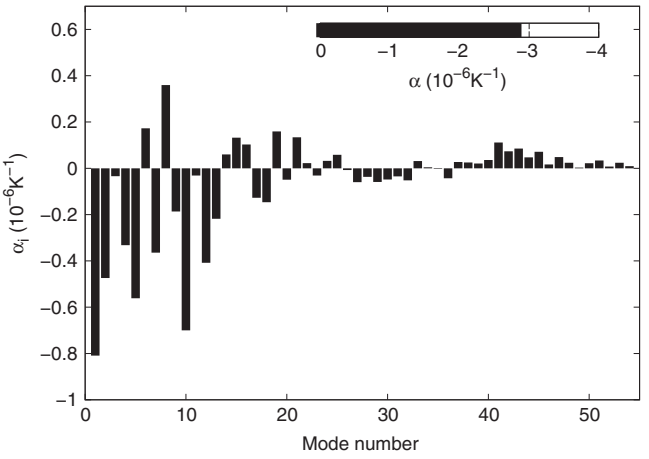

FIG. 2. Contribution of individual modes to the α-ZrW_2O_8 linear coefficient of thermal expansion at 300 K, within the Debye-Einstein model of the QHA. The inset at the top shows the overall CTE at 300 K.

on the basis of the present assignment and the data from Table I, that the infrared bands observed at 40, 75, and 100 cm^{-1} will shift to lower frequencies upon pressure increase.

In the quasiharmonic approximation, NTE arises from vibrational modes with negative mode Grüneisen parameters. Accordingly, the two lowest energy optic modes at 45 and 46 cm^{-1} (5.65 and 5.75 meV, respectively) contribute the most to NTE in α-ZrW_2O_8 at low temperature. In fact, within the Debye-Einstein QHA approximation, these two modes account for about 70% of the estimated CTE at 30 K. Their contribution remains important even at 300 K, as shown in Fig. 2. However, as temperature increases, other modes with energies up to 25 meV begin to contribute significantly to NTE in α-ZrW_2O_8. Although several modes above 25 meV exhibit negative mode Grüneisen parameters, their overall contribution to the room temperature CTE of α-ZrW_2O_8 is relatively small. An animated graphic is available in the Supplemental Material which shows how the individual vibrational modes contribute to the α-ZrW_2O_8 CTE as temperature increases [27].

To better understand the nature of the modes that most contribute to NTE in α-ZrW_2O_8, the variation in metal-metal and metal-oxygen bond lengths, inter- and intra-polyhedral bond angles, and polyhedral distortion was followed as each mode was scanned along its normal coordinates, using the computer program IVTON [29]. In these calculations, excursions along normal coordinates were restricted to ± 2 units of maximum classical displacement [24,30]. A detailed account of this analysis is available in the Supplemental Material [27].

The lowest energy optic modes at 45 and 46 cm^{-1} both exhibit some variation of intrapolyhedral O–*M*–O (*M* = Zr, W) bond angles, but only a slight variation in Zr–O1–W1 and Zr–O2–W2 interpolyhedral bond angles. Accordingly, in these modes the Zr$\cdots$W1 and Zr$\cdots$W2 distances remain almost constant, in very good

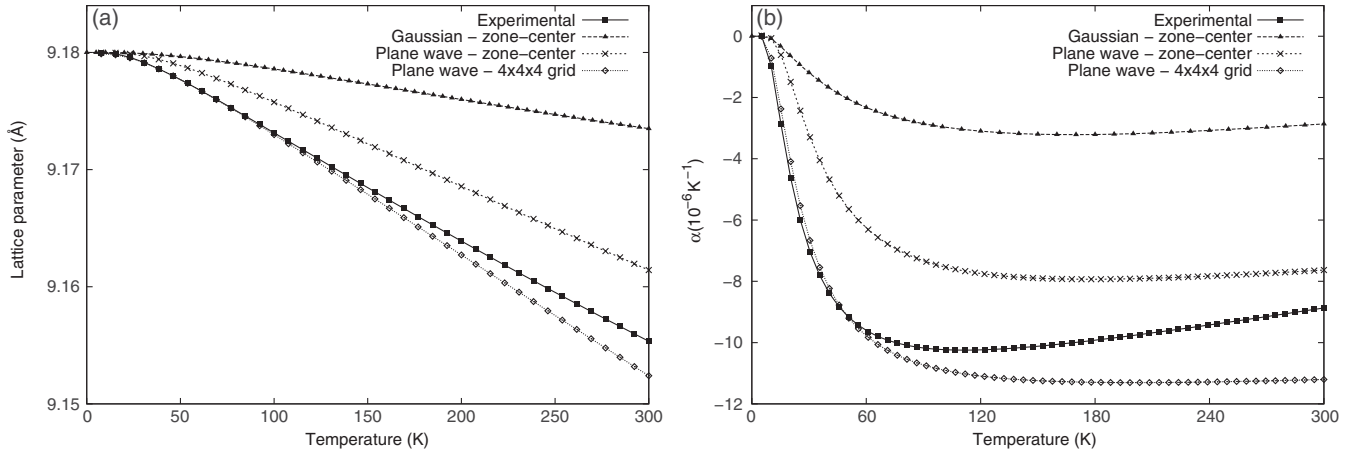

FIG. 3. Experimental and theoretical α-ZrW_2O_8 (a) lattice parameter and (b) linear CTE as a function of temperature. Gaussian–zone-center and plane wave–zone-center refer to results obtained within the Debye-Einstein model of the QHA from DFT calculations using atom-centered and plane wave basis sets, respectively. Plane wave–$4 \times 4 \times 4$ grid refers to results obtained with the inclusion of phonon dispersion. Theoretical results were all scaled to the experimental lattice parameter extrapolated to 0 K.

agreement with the conclusions drawn by Cao *et al.* from the analysis of $Zr \cdots W$ peaks in the Fourier transform of α-ZrW_2O_8 XAFS spectra [17,18]. Furthermore, in these modes the variation of intrapolyhedral bond angles occurs with minimal change of metal-oxygen bond lengths [31] and almost no polyhedral distortion (as defined in Ref. [32]), in a way compatible with the RUM model. This is accomplished by a large-amplitude librational and translational motion of the WO_4 units, which is made possible by the α-ZrW_2O_8 underconstrained framework structure. In fact, in the triply degenerated lowest energy optic mode, the bending of intrapolyhedral, transversal O1–Zr–O2 bonds, pushes the WO_4 tetrahedra back and forth along three equivalent directions nearly parallel to the $\langle 100 \rangle$ axis. As for the mode at 46 cm^{-1}, which shows almost no polyhedral distortion or variation in metal-oxygen bond length, the correlated motion of the WO_4 unit and its three neighbor ZrO_6 octahedra results in the translation of the tungsten tetrahedra, accompanied by the rocking motion of the terminal oxygen. The next zone-center mode, at 59 cm^{-1}, is very similar to the one previously described as the lowest energy mode by Hancock *et al.* [11], in which the bending of O1–Zr–O2 bonds and the rotation of ZrO_6 units makes the WO_4 polyhedra translate along the $\langle 111 \rangle$ axis. Animations representing the α-ZrW_2O_8 normal modes of vibration are available as a web page [33].

Figure 3 shows a comparison between the experimental and theoretical α-ZrW_2O_8 lattice parameters and the linear coefficients of thermal expansion as a function of temperature. The experimental CTE was obtained from the lattice parameter data of Evans *et al.* [9]. The α-ZrW_2O_8 lattice parameter dependence with temperature was found to be adequately described by $a(T) = a_0 + a_1 T^2 + a_2 T \exp(-a_3/T)$ [34]. The comparison between the experimental CTE and the theoretical estimate reveals that this latter accounts for about one third of the room temperature NTE in α-ZrW_2O_8. In order to assess the influence of the chosen calculation procedure on the estimate of the CTE, complementary plane wave pseudopotential calculations were performed using the Quantum Espresso suite [27,35]. The results, also shown in Fig. 3, suggest that the difference between experimental and theoretical results may be at least partially attributed to an underestimation of the mode Grüneisen parameters in the Becke three-parameter Lee-Yang-Parr hybrid functional calculations using atom-centered basis sets. Further inclusion of the effect of phonon dispersion, calculated from the frequencies of non-zone-center modes disposed in a uniform $4 \times 4 \times 4$ grid of q points, leads to a theoretical estimate for $a(T)$ in very good agreement with the experimental results up to about 60 K, as shown in Fig. 3. Above this temperature, the need for a more dense sampling of $\mathbf{q}$ space or, perhaps, the creation of thermal induced defects, may be responsible for the remaining difference between the theoretical and the experimental results. This preliminary account of the non-zone-center phonons also allowed the identification of several modes with very negative mode Grüneisen parameters, particularly the lowest acoustic modes at $\mathbf{q} = (1/4, 1/4, 1/4)$, halfway along the $\Gamma - R(\Lambda)$ line, and at $\mathbf{q} = (0, 0, 1/4)$, for which anomalous mode Grüneisen parameters around -80 were estimated.

Recently, NTE in ScF_3 has been attributed mainly to the anharmonicity of some vibrational modes that behave like quartic quantum oscillators [36]. Hence, a scanning of the α-ZrW_2O_8 zone-center optic modes along their respective normal coordinates was carried out to pinpoint any deviation from harmonic behavior. A simple harmonic potential fitted well the potential energy curve for the α-ZrW_2O_8 zone-center vibrational modes, as can be seen in the Supplemental Material [27]. Further work should be

devoted to scan the potential energy along the eigenvectors of the α-ZrW_2O_8 non-zone-center modes, particularly those with anomalous mode Grüneisen parameters, to search for possible similarities between the mechanisms behind NTE in ScF_3 and zirconium tungstate.

To conclude, by means of DFT calculations and within the Debye-Einstein model of the quasiharmonic approximation, we have identified the lowest energy optic modes at 45 and 46 cm^{-1}. Both of these modes have very negative mode Grüneisen parameters and thus contribute significantly to low temperature NTE in α-ZrW_2O_8. The complex nature of these modes exhibits features characteristic of both the rigid unit mode and the tent models. Other modes, particularly between 96 and 164 cm^{-1}, become increasingly important to α-ZrW_2O_8 NTE near room temperature. However, the contribution from modes with $E > 25$ meV to the room temperature α-ZrW_2O_8 CTE was shown to be relatively small. Further calculations are needed to extend this work and to fully explore the nature of the non-zone-center phonons more relevant to the NTE in zirconium tungstate, including the search for evidence of possible quartic oscillator behavior.

The authors acknowledge the computational support from CESUP (Centro Nacional de Supercomputação), Porto Alegre—RS and GridUCS (the computational grid of the Universidade de Caxias do Sul). This work was partially supported by the Brazilian agencies CNPq (Conselho Nacional de Desenvolvimento Científico e Tecnológico) and FAPERGS (Fundação de Amparo à Pesquisa do Estado do Rio Grande do Sul).

*caperott@ucs.br

[1] C. Martinek and F. A. Hummel, J. Am. Ceram. Soc. **51**, 227 (1968).
[2] J. Graham, A. D. Wadsley, J. H. Weymouth, and L. S. Williams, J. Am. Ceram. Soc. **42**, 570 (1959).
[3] T. A. Mary, J. S. O. Evans, T. Vogt, and A. W. Sleight, Science **272**, 90 (1996).
[4] A. K. A. Pryde, K. D. Hammonds, M. T. Dove, V. Heine, J. D. Gale, and M. C. Warren, J. Phys. Condens. Matter **8**, 10 973 (1996).
[5] A. K. A. Pryde, K. D. Hammonds, M. T. Dove, V. Heine, J. D. Gale, and M. C. Warren, Phase Transit. **61**, 141 (1997).
[6] G. Ernst, C. Broholm, G. R. Kowach, and A. P. Ramirez, Nature (London) **396**, 147 (1998).
[7] A. P. Ramirez and G. R. Kowach, Phys. Rev. Lett. **80**, 4903 (1998).
[8] W. I. F. David, J. S. O. Evans, and A. W. Sleight, Europhys. Lett. **46**, 661 (1999).
[9] J. S. O. Evans, T. A. Mary, T. Vogt, M. A. Subramanian, and A. W. Sleight, Chem. Mater. **8**, 2809 (1996).
[10] K. Wang and R. R. Reeber, Appl. Phys. Lett. **76**, 2203 (2000).
[11] J. N. Hancock, C. Turpen, Z. Schlesinger, G. R. Kowach, and A. P. Ramirez, Phys. Rev. Lett. **93**, 225501 (2004).
[12] R. Mittal, S. L. Chaplot, H. Schober, and T. A. Mary, Phys. Rev. Lett. **86**, 4692 (2001).
[13] R. Mittal and S. L. Chaplot, Phys. Rev. B **60**, 7234 (1999).
[14] T. R. Ravindran, A. K. Arora, and T. A. Mary, Phys. Rev. Lett. **84**, 3879 (2000).
[15] S. L. Chaplot and R. Mittal, Phys. Rev. Lett. **86**, 4976 (2001).
[16] T. R. Ravindran and A. K. Arora, Phys. Rev. Lett. **86**, 4977 (2001).
[17] D. Cao, F. Bridges, G. R. Kowach, and A. P. Ramirez, Phys. Rev. Lett. **89**, 215902 (2002).
[18] D. Cao, F. Bridges, G. R. Kowach, and A. P. Ramirez, Phys. Rev. B **68**, 014303 (2003).
[19] M. G. Tucker, A. L. Goodwin, M. T. Dove, D. A. Keen, S. A. Wells, and J. S. O. Evans, Phys. Rev. Lett. **95**, 255501 (2005).
[20] B. Fultz, Prog. Mater. Sci. **55**, 247 (2010).
[21] M. T. Dove, *Introduction to Lattice Dynamics* (Cambridge University Press, Cambridge, England, 1993), p. 76.
[22] J. L. Fleche, Phys. Rev. B **65**, 245116 (2002).
[23] A. Otero-de-la-Roza, D. Abbasi-Pérez, V. Luaña, Comput. Phys. Commun. **182**, 2232 (2011).
[24] R. Dovesi *et al.*, *CRYSTAL2006 User's Manual* (University of Torino, Torino, Italy, 2006).
[25] A. D. Becke, J. Chem. Phys. **98**, 5648 (1993).
[26] C. A. Figueirêdo and C. A. Perottoni, Phys. Rev. B **75**, 184110 (2007).
[27] See Supplemental Material at http://link.aps.org/supplemental/10.1103/PhysRevLett.109.195503 for details of the computational first-principles calculations, the optimized lattice parameter and atomic positions, a plot of normal mode wave number versus pressure, an animation showing the contribution of individual modes to the α -ZrW_2O_8 linear coefficient of thermal expansion as a function of temperature, and the variation of bond lengths, bond angles, and potential energy as the crystal structure of α-ZrW_2O_8 follows along each normal mode coordinate.
[28] A. P. Scott and L. Radom, J. Phys. Chem. **100**, 16 502 (1996).
[29] T. Balic Zunic and I. Vickovic, J. Appl. Crystallogr. **29**, 305 (1996).
[30] The maximum classical displacement corresponds to the distance from the origin in which the potential energy in the harmonic approximation equals the energy of the vibrational mode.
[31] The variation is less than 0.3% for the worst case, the change of W1–O1 bond length for a displacement of two units of maximum classical displacement along the 45 cm^{-1} normal mode coordinate.
[32] E. Makovicky and T. Balic-Zunic, Acta Crystallogr. Sect. B **54**, 766 (1998).
[33] A web page displaying animations of α-ZrW_2O_8 normal modes can be found at http://www.ucs.br/ccet/defq/caperott/vib.html.
[34] J. B. Wachtman, Jr., W. E. Tefft, D. G. Lam, Jr., and C. S. Apstein, Phys. Rev. **122**, 1754 (1961).
[35] P. Giannozzi *et al.*, J. Phys. Condens. Matter **21**, 395502 (2009).
[36] C. W. Li, X. Tang, J. A. Muñoz, J. B. Keith, S. J. Tracy, D. L. Abernathy, and B. Fultz, Phys. Rev. Lett. **107**, 195504 (2011).